

**Dangling bonds and vacancies in germanium**J. R. Weber,<sup>1</sup> A. Janotti,<sup>2</sup> and C. G. Van de Walle<sup>2</sup><sup>1</sup>*Department of Physics, University of California, Santa Barbara, California 93106-9530, USA*<sup>2</sup>*Materials Department, University of California, Santa Barbara, California 93106-5050, USA*

(Received 3 October 2011; revised manuscript received 19 November 2012; published 14 January 2013)

The quest for metal-oxide-semiconductor field-effect transistors (MOSFETs) with higher carrier mobility has triggered great interest in germanium-based MOSFETs. Still, the performance of germanium-based devices lags significantly behind that of their silicon counterparts, possibly due to the presence of defects such as dangling bonds (DBs) and vacancies. Using screened hybrid functional calculations we investigate the role of DBs and vacancies in germanium. We find that the DB defect in germanium has no levels in the band gap; it acts as a negatively charged acceptor with the  $(0/-1)$  transition level below the valence-band maximum (VBM). This explains the absence of electron-spin-resonance observations of DBs in germanium. The vacancy in germanium has a much lower formation energy than the vacancy in silicon and is stable in a number of charge states, depending on the position of the Fermi level. We find the  $(0/-1)$  and  $(-1/-2)$  transition levels at 0.16 and 0.38 eV above the VBM; the spacing of these levels is explained based on the strength of intraorbital repulsion. We compare these results with calculations for silicon, as well as with available experimental data.

DOI: [10.1103/PhysRevB.87.035203](https://doi.org/10.1103/PhysRevB.87.035203)

PACS number(s): 61.72.uf, 71.55.Cn, 85.30.Tv

**I. INTRODUCTION**

Germanium is a promising material for use in the channel of novel complementary metal-oxide semiconductor (CMOS) devices. It would enable transistors with higher channel mobilities than those in standard silicon CMOSs and allow for lower voltage operation, due to its significantly smaller band gap.<sup>1</sup> Existing *p*-channel germanium-based MOSFETs show acceptable performance, although they exhibit an undesirable positive threshold voltage shift.<sup>2,3</sup> *n*-channel MOSFETs have been less successful, suffering from low channel mobilities and on-state currents.<sup>4-6</sup> The poor device performance is likely caused by the presence of defects near the semiconductor-dielectric interface, such as germanium dangling bonds (DBs) or vacancies, making the study and characterization of these defects a much needed and timely task.

Numerous experimental techniques are available for studying defects in semiconductors. In particular, electron-spin resonance (ESR) has been successful in the characterization of defects in a wide range of semiconductor materials.<sup>7</sup> Capable of detecting defect states with unpaired electrons, ESR studies indicate that interfacial DB defects play a very different role at germanium-oxide interfaces<sup>8</sup> compared to their silicon counterpart.<sup>9,10</sup> ESR has been used extensively to characterize DB defects at silicon-oxide interfaces<sup>9,10</sup> but has been unable to detect germanium DBs at germanium-oxide interfaces.<sup>8</sup> Germanium DBs do become detectable when germanium is alloyed with silicon<sup>11-14</sup> (7-55% silicon). Various explanations have been proposed to explain this result, and they fall into two main categories: one is based on stress, the other on the position of the germanium DB levels.

One proposal is that the DB concentration strongly varies with stress at the interface, being very low for pure germanium and increasing when silicon is added.<sup>11-15</sup> The effect of stress on DB concentration was studied in detail at Si-SiO<sub>2</sub> interfaces.<sup>9</sup> By varying the oxidation temperature, which effectively controls the stress at the interface, the DB concentration at Si-SiO<sub>2</sub> interfaces was found to vary from 10<sup>13</sup> to less than 10<sup>10</sup> DBs per cm<sup>2</sup>. Similar studies cannot be performed at

germanium-oxide interfaces since the germanium DBs cannot be detected, so the suggestion that stress plays a role is based on an assumed analogy with silicon.

Another proposed explanation for the absence of an ESR signal is that the DBs are always present but that the energetic position of the corresponding defect level is such that they elude detection by ESR.<sup>16-19</sup> Within this category, results and interpretations for the precise position of the DB level vary. One result (previous work by the present authors) finds the DB levels well below the valence-band maximum (VBM),<sup>16</sup> while others find the levels within the band gap, though close enough to the VBM to reduce the concentration of neutral DBs (the charge state detectable by ESR) below the detectable limit.<sup>17-19</sup>

Calculations based on density-functional theory (DFT), as well as many-body perturbation theory within the  $G_0W_0$  approximation, found the DB levels in germanium to be positioned more than 0.4 eV below the VBM.<sup>16</sup> This implies that the germanium DBs cannot be detected in ESR experiments because they are always negatively charged (doubly occupied) for any value of the Fermi level. Other studies, using the PBE0 hybrid functional proposed by Perdew, Burke, and Ernzerhof,<sup>20</sup> found the germanium DB levels to be just above the VBM, with the neutral charge state stable in a very narrow range of 0.06 eV.<sup>17-19</sup> The authors of those studies argued that even though the DB levels were located above (but close to) the VBM the ESR signal would be significantly attenuated due to the presence of valence-band tail states, which would broaden the DB levels, thus reducing the overall observed neutral DB concentration.<sup>17-19</sup>

In addition to DBs, it is also important to investigate the properties of vacancies in germanium, since they have been predicted to have a much lower formation energy and thus occur in much higher concentrations than in silicon.<sup>21</sup> Calculations published to date have shown inconsistent results.<sup>21-23</sup> The discrepancy can probably be attributed to the different approximations made within the DFT framework. Conventional DFT calculations within the local-density approximation (LDA) or generalized gradient approximation (GGA)

underestimate the band gap, even predicting germanium to be a semimetal.<sup>24</sup> In previous studies, different methods of varying sophistication were employed to correct the germanium band gap, resulting in conflicting results for the position of the vacancy levels.<sup>21–23</sup> In the study by Fazio *et al.*,<sup>21</sup> modifications were made to the germanium pseudopotential, while Śpiewak *et al.*<sup>22</sup> employed LDA +  $U$  and Tahini *et al.*<sup>23</sup> used GGA +  $U$ .

Vacancies in germanium have been studied by ESR,<sup>25</sup> Hall measurements,<sup>26–28</sup> positron annihilation spectroscopy,<sup>29</sup> perturbed angular correlation spectroscopy (PACS),<sup>30,31</sup> and deep level transient spectroscopy (DLTS).<sup>32</sup> Of these techniques, PACS and DLTS have provided the most detailed insight into the defect levels associated with the vacancy.<sup>30,31</sup> Both of these methods allow for the study of the charge state of the defect as a function of Fermi-level position, thereby providing information on the defect transition levels. Two charge-state transition levels have been associated with the germanium vacancy. The first is related to the  $(0/-1)$  transition level and was found to be  $0.2 \pm 0.04$  eV above the VBM.<sup>30,31</sup> The second level, which has not been explicitly associated with a specific charge-state transition, was found at 0.33 eV above the VBM.<sup>32</sup> These results are at odds with the predictions of the DFT calculations by Fazio *et al.*,<sup>21</sup> who found the  $(0/-1)$  transition level above midgap,<sup>21</sup> while Śpiewak *et al.*<sup>22</sup> found this level just above the VBM. The recent GGA +  $U$  results of Tahini *et al.*,<sup>23</sup> in which the germanium band gap is 0.67 eV and close to the experimental value, place the  $(0/-1)$  level at 0.24 eV, in agreement with experiment. Still, as we will argue in Sec. III C, even the GGA +  $U$  calculations fall short in describing other transition levels.

In this study we use a more advanced functional within DFT to address the properties of DBs and vacancies in germanium. Specifically, we use a screened hybrid functional which provides an accurate description of the band structure and has been successful in predicting the properties of defects and impurities in various materials.<sup>33–35</sup> In the sections that follow we will describe the computational approach, present our results, and provide a detailed comparison with experimental data as well as with similar defects in silicon.

## II. COMPUTATIONAL APPROACH

The calculations presented here are based on a generalized Kohn-Sham scheme<sup>36</sup> utilizing the screened hybrid functional of Heyd, Scuseria, and Ernzerhof (HSE),<sup>37,38</sup> as implemented in the VASP code.<sup>39–42</sup> The amount of Hartree-Fock exchange (mixing parameter) included was chosen to accurately describe the band gaps of Si and Ge. For silicon, we used the standard 25% Hartree-Fock exchange; for Ge, 30% Hartree-Fock exchange is needed to achieve the correct band gap. Projector-augmented wave potentials<sup>40,43</sup> with four valence electrons were used for both Si and Ge. Spin polarization was also included.

Defects were modeled by adding (removing) atoms to (from) a germanium crystal geometry with periodic boundary conditions. Calculations were performed using 64- and 216-atom supercells for both the dangling bond and vacancy. We utilized a plane-wave basis set truncated at 250 eV, with special  $k$  points for integration over the Brillouin zone: a  $2 \times 2 \times 2$

grid for 64-atom supercells and the  $\Gamma$  point for 216-atom supercells. The different supercell sizes allowed us to study the error introduced by spurious defect-defect interactions.

### A. Formation energies and defect concentrations

In thermodynamic equilibrium and in the dilute regime, the concentration of a defect is related to the formation energy ( $E^f$ ) through a Boltzmann relation:<sup>44</sup>

$$C = N_0 e^{-E^f/k_B T}, \quad (1)$$

where  $N_0$  is the number of possible defect sites and  $k_B T$  is the temperature in eV. This expression shows that as the formation energy of a defect increases the concentration decreases exponentially. The formation energy ( $E^f$ ) of a defect is not simply a constant. It depends on the Fermi level ( $\varepsilon_F$ ) in the material, which is the energy of the electron reservoir or the electron chemical potential. For example, the formation energy of a germanium vacancy in charge state  $q$  ( $V_{\text{Ge}}^q$ ) is given by the following expression:

$$E^f[V_{\text{Ge}}^q] = E_{\text{tot}}[V_{\text{Ge}}^q] - E_{\text{tot}}[\text{Ge}] + \mu_{\text{Ge}} + q\varepsilon_F. \quad (2)$$

The  $E_{\text{tot}}$  terms are the total energies of the germanium crystal with and without the  $V_{\text{Ge}}^q$  defect, and the chemical potential  $\mu_{\text{Ge}}$  is the energy per atom of bulk germanium. The Fermi level ( $\varepsilon_F$ ) is referenced to the bulk VBM. The position of the bulk VBM with respect to the defect supercell was obtained through the alignment of the averaged electrostatic potential in a bulklike region of the defect supercell.<sup>44</sup> This alignment procedure provides an implicit charge-state correction to the formation energies.<sup>44</sup> Convergence checks as a function of supercell size will be discussed in Sec. III. We have also investigated the effect of charge-state corrections based on the scheme of Freysoldt *et al.*,<sup>45</sup> which includes a more rigorous treatment of the electrostatic problem. This scheme resulted in formation energies and charge-state transition levels that typically differed by less than 0.1 eV from the values based on potential alignment. We observed, however, that for the sizes of supercells employed here some wave-function overlap cannot be excluded, which (as discussed in Ref. 45) introduces uncertainty in the correction scheme. We therefore elected to employ the potential-alignment approach for the results presented in the paper. Spin-orbit splitting of the valence band was included. The Fermi level in Eq. (2) is a variable, and it is instructive to examine formation energies of point defects as functions of  $\varepsilon_F$ . In practice, one plots the formation energy allowing  $\varepsilon_F$  to vary from the VBM to the conduction-band minimum (CBM).

### B. Defect transition levels

In semiconductors and insulators, defects typically introduce levels in the band gap.<sup>7,46,47</sup> These levels involve transitions between different charge states of the same defect and can be derived from the calculated formation energies. The charge-state transition level ( $q/q'$ ) is defined as the Fermi-level position for which the formation energies of two different charge states  $q$  and  $q'$  of a defect are equal, i.e.,

$$(q/q') = -\frac{E^f(D^q; \varepsilon_F = 0) - E^f(D^{q'}; \varepsilon_F = 0)}{q - q'}. \quad (3)$$

$E^f(D^q; \varepsilon_F = 0)$  is the formation energy of the defect  $D$  in the charge state  $q$  when the Fermi level is at the VBM ( $\varepsilon_F = 0$ ). For  $\varepsilon_F$  below ( $q/q'$ ), the defect has a charge  $q$ , while for  $\varepsilon_F$  above ( $q/q'$ ) the defect has a charge  $q'$ . These transition levels can be observed using experimental techniques such as DLTS or PACS. The location of such levels can impact semiconductor device performance, since the charge state of defects will be determined by both the position of the defect levels and the Fermi level in the material.

### C. Modeling a dangling bond

The geometries used for electronic structure calculations of point defects are typically straightforward to construct. For example, constructing a crystal with a germanium vacancy is as simple as removing a single germanium atom from the bulk crystal. Modeling an isolated DB is more complicated, however. DBs occur in a variety of atomic configurations: at interfaces, on surfaces, and in point defects such as vacancies. Explicit calculations for germanium-oxide interfaces are challenging and would lead to an array of different defect configurations, rendering it difficult to extract generic properties of the DB. Similar problems exist on surfaces, due to surface reconstructions. Additional complications can arise, since DBs which occur on a specific surface reconstruction usually interact, leading to the formation of a band rather than an isolated defect level. Such DB interactions are even stronger in the case of vacancies, where in the case of tetrahedrally bonded semiconductors the DB levels are known to give rise to  $a_1$  and  $t_2$  levels that can be separated by a large energy, indicative of the strength of the interaction.<sup>7,46,47</sup>

Therefore we have resorted to a specific geometry that enables us to study an isolated DB in germanium, as illustrated in Fig. 1. It is generated by creating a small void inside the crystal, specifically by removing four germanium atoms. One can imagine first creating a single vacancy, then removing three of the germanium atoms that neighbor the vacancy. This

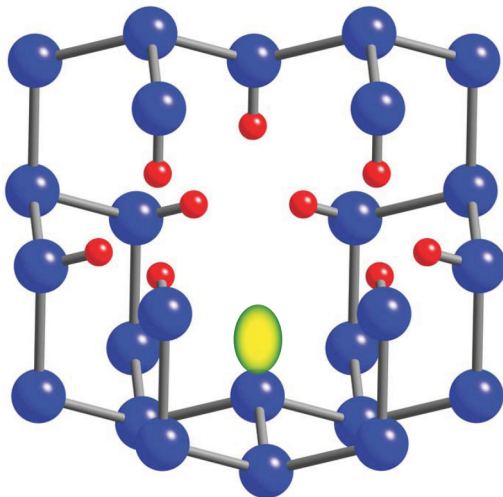


FIG. 1. (Color online) Schematic representation of the structure used to study an isolated DB, as described in the text. Large blue spheres represent germanium atoms, and small red spheres represent hydrogen atoms. The yellow oval represents the isolated DB.

generates nine DBs, which are far removed from the DB on the atom neighboring the original vacancy that we did not remove.

These nine DBs can then be passivated with hydrogen, leaving behind a single isolated germanium DB. The Ge–H bond distances were optimized through structural relaxations. These Ge–H bonds will of course contribute to the total energy of the entire structure. However, all of our relevant results can be obtained as energy differences in which these contributions cancel, since we keep the atomic configurations of these nine Ge–H bonds fixed in all calculations. This approach will not yield a formation energy that is directly related to DB concentration through Eq. (1), since the void is an artificial construction. However, the charge-state transition levels that we extract from these calculations do represent the energy required to add (remove) electrons to (from) the DB. This procedure has been previously used to study DBs in silicon<sup>48</sup> and aluminum oxide.<sup>49</sup>

## III. RESULTS AND DISCUSSION

### A. Bulk properties

The germanium crystal has the diamond structure, with a lattice constant of 5.65 Å.<sup>50</sup> Using the screened hybrid functional, we find a value of 5.69 Å, within 1% of the experimental value. A two-atom unit cell with  $8 \times 8 \times 8$   $k$ -point sampling was used for bulk calculations. The results for the lattice parameter and bulk modulus using PBE and HSE are shown in Table I, indicating good agreement between HSE and experiments and that increasing the Hartree-Fock mixing parameter to 30% from the standard 25% value has only a small effect on bulk properties.

The amount of Hartree-Fock exchange interaction included in the hybrid functional (30%) was selected to match the experimental indirect band gap ( $E_g^L$ ). Table II illustrates this agreement. The direct gap ( $E_g^\Gamma$ ) is smaller than experiment by 0.14 eV, while the  $\Gamma$ -X indirect band gap ( $E_g^X$ ) is larger by 0.33 eV (note that an experimental  $T = 0$  value of the gap at X does not seem to be available). These deviations from the experimental band structure at higher-lying band extrema are not expected to affect our defect calculations. In Fig. 2 we have plotted the band structure along the L- $\Gamma$ -X path. For Si, the calculated value of the fundamental band gap (with the CBM on the  $\Gamma$ -X line) is 1.14 eV, using the standard 25% mixing in the HSE functional.

TABLE I. Calculated and experimental<sup>50</sup> values for lattice parameter, bulk modulus, and cohesive energy of germanium. Results for PBE and HSE with Hartree-Fock mixing of 30% are shown for comparison.

Method	Lattice parameter (Å)	Bulk modulus (G Pa)	Cohesive energy (eV)
PBE	5.780	64.5	-3.741
HSE (25%)	5.703	83.6	-3.721
HSE (30%)	5.690	83.1	-3.722
Exp.	5.658	75.8	-3.85

TABLE II. Calculated and experimental<sup>50</sup> band gaps of germanium. All values are 0-K extrapolations, except for  $E_g^X$ , which is a room-temperature value. The calculated values are obtained using the HSE hybrid functional with a mixing parameter of 30%.

Band gap	Calc. (eV)	Exp. (eV)
$E_g^L$	0.74	0.74
$E_g^\Gamma$	0.75	0.89
$E_g^X$	1.53	1.20

### B. Dangling bond

We investigate the properties of the DB in germanium by calculating the associated charge-state transition levels. To do so, we need to first calculate the formation energy for a DB in charge state  $q$  ( $DB^q$ ), which we define as follows:

$$E^f[\text{Ge} : DB^q] = E_{\text{tot}}[\text{Ge} : DB^q] - E_{\text{tot}}[\text{Ge} : DB + H] + \mu_H + q\varepsilon_F. \quad (4)$$

The  $E_{\text{tot}}$  terms are the total energies of the germanium crystal with the charged DB ( $DB^q$ ), and the DB passivated with hydrogen ( $DB+H$ ). The  $\mu_H$  term refers to the hydrogen chemical potential; we used an isolated  $H_2$  molecule as a reference. The remaining terms are identical to those discussed previously in Eq. (2). The DB can be occupied with zero, one, or two electrons, corresponding to charge states  $q = +1, 0$ , or  $-1$ , respectively.

In Fig. 3, we have plotted the formation energy as a function of Fermi level. In this plot we show only the charge state with the lowest formation energy for each value of Fermi level. Analyzing Fig. 3, we find two charge-state transition levels, both of which are below the germanium VBM. The  $(+1/0)$  level is at  $-0.21$  eV and the  $(0/-1)$  level is at  $-0.11$  eV, referenced to the VBM. This result is in qualitative agreement with our previous computational study on the germanium DB,<sup>16</sup> which also found the associated DB levels to be below the germanium VBM, but quantitative differences occur: the present levels are higher in energy by about 0.3 eV. In addition, the previous study found the DB to be a negative- $U$  defect,<sup>51</sup> meaning that the  $(0/-)$  transition level was below the  $(+/0)$  level. The present results find the  $(0/-)$  level above the  $(+/0)$  level, meaning that in principle the neutral charge state of the

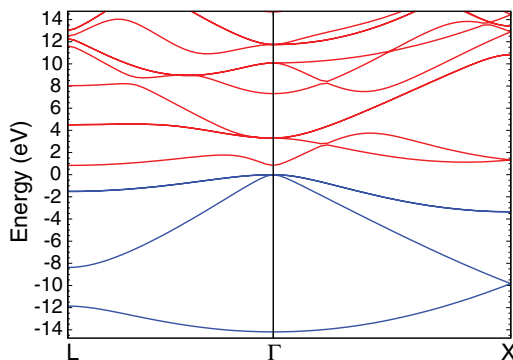


FIG. 2. (Color online) Calculated band structure of germanium. Blue lines represent valence bands, and red lines represent conduction bands. The zero of energy is set at the VBM.

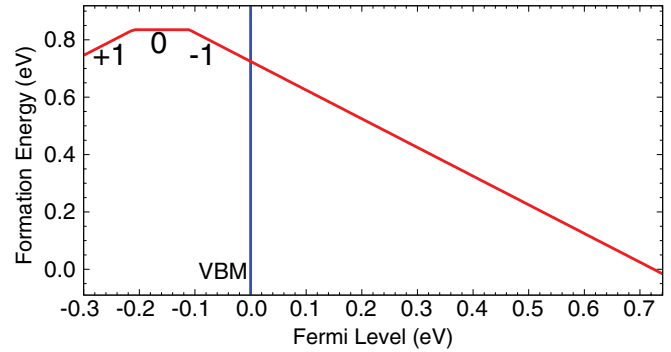


FIG. 3. (Color online) Calculated formation energy of the DB in germanium. The Fermi level is referenced to the VBM.

DB would be stable over a range of Fermi levels about 0.1 eV wide and centered at  $-0.16$  eV. In practice, of course, the Fermi level (or quasi-Fermi level) can never be pushed that far below the VBM. Both our previous<sup>16</sup> and present calculations thus agree that the dangling bond can only occur in the negative charge state. The neutral charge state, which would be required to make the defect paramagnetic, can never be stabilized and thus observations of the DB by ESR are impossible.

In silicon, the neutral DB is of course stable; i.e., the  $(0/-)$  transition level occurs within the band gap. This was indeed confirmed through calculations, as illustrated in Fig. 4. If we assume that the germanium DB level remains constant on an absolute energy scale as the alloy concentration is changed, which is a reasonable assumption for a highly localized state, we can use the valence-band offset between silicon and germanium [calculated, 0.6 eV;<sup>52</sup> experiment, 0.55 eV (Ref. 53)] to estimate the position of the germanium DB level in pure silicon; this estimate leads to a value for the germanium DB  $(0/-)$  level of 0.49 eV above the silicon VBM. Interpolating between the position of this level in silicon and germanium then provides an estimate of the silicon concentration in a  $Si_{1-x}Ge_x$  alloy at which the level would cross the VBM and

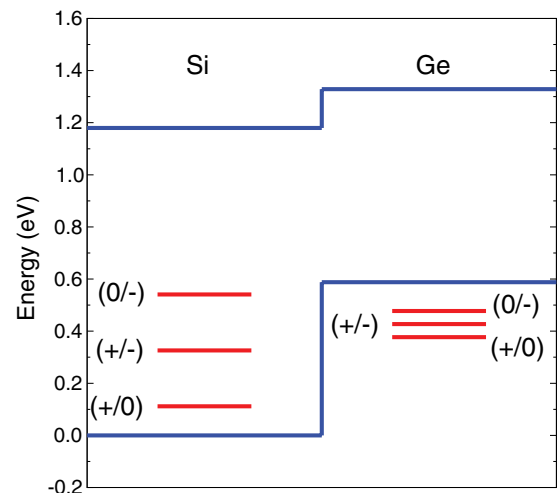


FIG. 4. (Color online) Calculated DB charge-state transition levels for the germanium and silicon DBs. The alignment of the band structures is based on the calculated valence-band offset of 0.6 eV.<sup>51</sup>

hence become observable as a function of increasing silicon concentration. Our results indicate that this would occur at  $x = 0.82$ , i.e., a silicon concentration of 18%, in reasonable agreement with the 7% silicon concentration that was found to be necessary to detect the DB by ESR in the experiments of Refs. 11–13.

Experimentally, the ESR signal from  $\text{Si}_{1-x}\text{Ge}_x\text{-SiO}_2$  interfaces<sup>11–14</sup> was analyzed as a function of germanium concentration  $x$  in the alloy, and the results were used to provide an estimate of where the germanium-DB-related defect levels would lie if referenced to the silicon band gap. They were found to be located at  $0.35 \pm 0.10$  eV above the silicon VBM.<sup>14</sup> Again assuming that the germanium DB level remains constant on an absolute energy scale as the alloy concentration is changed, we can estimate the position of the germanium DB levels in pure germanium. The resulting estimate, at  $0.25 \pm 0.10$  eV below the germanium VBM, is within 0.1 eV of our present results (and would be even closer if the smaller valence-band offset reported in Ref. 14 were used). We can conclude that our results are in very good agreement with the available experimental data.

We now discuss the comparison with the results of Broqvist *et al.*, who found the germanium DB levels to be located just above the VBM,<sup>17–19</sup> with the (+1/0) transition level at 0.05 eV and the (0/−1) level at 0.11 eV above the VBM. Broqvist *et al.* also used a hybrid functional approach, but the specific functional was different: they used the PBE0 functional,<sup>20</sup> which does not contain the screening of the Hartree-Fock exchange interaction included in our approach. We prefer to include screening effects; however, we feel that the choice of the specific hybrid functional should lead to only minor differences in the position of the transition levels. A more significant effect may be due to the choice of supercell, which translates into different degrees of Brillouin-zone folding in reciprocal space. For defect states near or below the VBM, special care has to be taken when occupying the state with a specific number of electrons to describe the various charge states of the defect. In the calculations presented above, we used a grid of special  $k$  points that is shifted away from  $\Gamma$  within a 64-atom supercell.

We also performed calculations for a 216-atom supercell (the same geometry as used by Broqvist *et al.* Refs. 17–19). Calculations for the negative charge state, in which the DB state is completely occupied, are straightforward and lead to formation energies very similar (to within 0.07 eV) of the results obtained with the 64-atom cell. We found calculations for the neutral or positive charge state to be very difficult to perform, however. Due to Brillouin-zone folding, the DB state strongly mixes with host states near the VBM, creating an ambiguity as to which state is actually associated with the DB. If we simply remove electrons from the highest occupied state we are likely to underestimate the energy of the neutral and positive charge states, resulting in transition levels that are too high in energy. This problem persists, in a 216-atom cell, even if we use special  $k$  points shifted away from the  $\Gamma$  point. We therefore feel that the 64-atom cell calculations, in which the defect state at the special  $k$  points is well separated from the VB states (due to a lesser amount of Brillouin-zone folding), are more reliable because of the unambiguous occupation of the defect state with different numbers of electrons. The results

reported in Fig. 3 are for the 64-atom calculation. We feel that the slightly higher values for the germanium DB transition levels obtained by Broqvist *et al.*<sup>17–19</sup> may be due to their use of a 216-atom supercell. Another possibility is that the VBM is slightly lower within the PBE0 formalism, compared with our approach. In addition, our choice of a 64-atom supercell seems reasonable since we found the formation energy of silicon DBs in both the 64- and 216-atom supercells to vary by only 0.09 eV.

Our results indicate that the DB in germanium is always negatively charged, regardless of the position of the Fermi level. As noted above, this explains the absence of an observed ESR signal, which relies on unpaired electrons (stability of a neutral charge state). The negative charge on the germanium DB also has important consequences for MOS-based devices. DB defects near an interface will give rise to fixed negative charge, creating serious problems for devices that rely on the formation of an electron channel (such as  $n$ -channel MOSFETs).<sup>54</sup> Even for  $p$ -channel devices, such a fixed charge may create undesirable carrier scattering, as well as a positive threshold voltage shift.<sup>2,3</sup> Finally, we note that hydrogen passivation of these DB defects, which is a very successful procedure at Si-SiO<sub>2</sub> interfaces, is expected to be inefficient in germanium. We have previously shown that hydrogen acts exclusively as an acceptor in germanium,<sup>16,55</sup> and hence electrostatic repulsion between the DB and hydrogen impurities will suppress passivation of these DBs by hydrogen, consistent with experimental observations showing the absence of any improvement upon hydrogenation.<sup>8</sup>

## C. Vacancy

### 1. Electronic structure of the germanium vacancy

The electronic structure of the vacancy can be understood as follows: the four DBs on neighboring germanium atoms interact strongly and give rise to a symmetric  $a_1$  state deep in the valence band and three degenerate  $t_2$  states in the gap.<sup>7,46,47</sup> The occupancy of these defect states along with the associated atomic relaxations determine the formation energy of the vacancy. The calculated formation energy of the germanium vacancy as a function of Fermi level is shown in Fig. 5. Our convergence tests indicated that a 216-atom supercell was necessary to obtain reliable results in the case of the vacancy, because, just as in silicon,<sup>56</sup> the  $t_2$  states associated

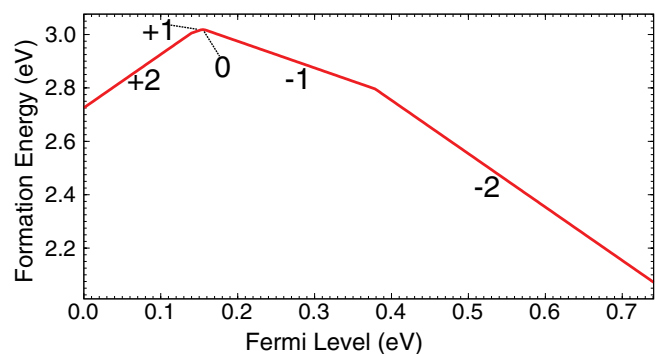


FIG. 5. (Color online) Calculated formation energy of the vacancy in germanium. The Fermi level is referenced to the VBM.

TABLE III. Calculated lowest-energy spin states corresponding to each charge state of the vacancy.

Charge state	Spin state
+2	0
+1	1/2
0	1
-1	3/2
-2	1

with the defect are quite delocalized along the (110) direction and cannot be reliably described within a 64-atom supercell. Similar results showing delocalization of vacancy states were observed by Fazzio *et al.*<sup>21</sup> Spin-polarized calculations were used to determine the lowest-energy spin state corresponding to each charge state of the vacancy, as shown in Table III.

In the neutral charge state of the vacancy, four electrons (one from each germanium DB) are available to fill the vacancy-induced single-particle Kohn-Sham states. Two electrons go into the  $a_1$  state and two are left to occupy the  $t_2$  states. Upon adding one additional electron to obtain the -1 charge state, all of the  $t_2$  states become occupied with one electron, as shown in Fig. 6. The -1 charge state therefore results in a spin-3/2 configuration. The schematic of single-particle states shown in Fig. 6 provides physical insight into the formation of the +2, +1, 0, and -1 charge states and the corresponding transition levels. In the +2 charge state, the  $t_2$  states are unoccupied (note that the  $a_1$  states, which are well below the VBM, are always occupied, and hence the +2 charge state is the lowest achievable charge state of the vacancy). Adding one, two, or three electrons to the spin-majority channel of the  $t_2$  vacancy states results in the +1, 0, and -1 charge states. The corresponding calculated values of the (+2/+1), (+1/0), and (0/-1) charge-state transition levels are listed in Table IV.

Starting from the -1 charge state, the -2 charge state is obtained by adding an additional electron, which must occupy

TABLE IV. Calculated charge-state transition levels associated with the germanium vacancy.

Transition level	Energy (eV)
(+2/+1)	0.14
(+1/0)	0.15
(0/-1)	0.16
(-1/-2)	0.38

the empty spin-minority channel associated with the  $t_2$  states. This leads to a significant rearrangement of the single-particle states, as shown in Fig. 7.

The additional electron introduces an intraorbital electron-electron repulsion between the two electrons in the  $t_2$  state that is doubly occupied, explaining the large separation between the (0/-1) and (-1/-2) charge-state transition levels (see Fig. 5 and Table IV). The magnitude of this separation, compared to the modest separation between the (+2/+1), (+1/0), and (0/-1) transition levels, indicates that intraorbital repulsion is a much stronger effect than interorbital repulsion. The higher position of the (-1/-2) level leads to a larger range of Fermi level for which the -1 charge state is stable.

Experimental techniques such as PACS and DLTS have been used to probe these defect levels. PACS measurements have found the (0/-1) transition level to be at  $0.2 \pm 0.04$  eV above the VBM,<sup>30,31</sup> in very good agreement with our calculated value of 0.16 eV. DLTS experiments have found a level associated with the vacancy to be located at 0.33 eV above the VBM.<sup>32</sup> Those experiments did not determine which charge states were involved in this transition. We note that this level is close to our calculated value for the (-1/-2) transition level at 0.38 eV above the VBM.

## 2. Comparison with previous calculations

We now compare our results to the three previously published computational studies for the germanium vacancy.<sup>21-23</sup>

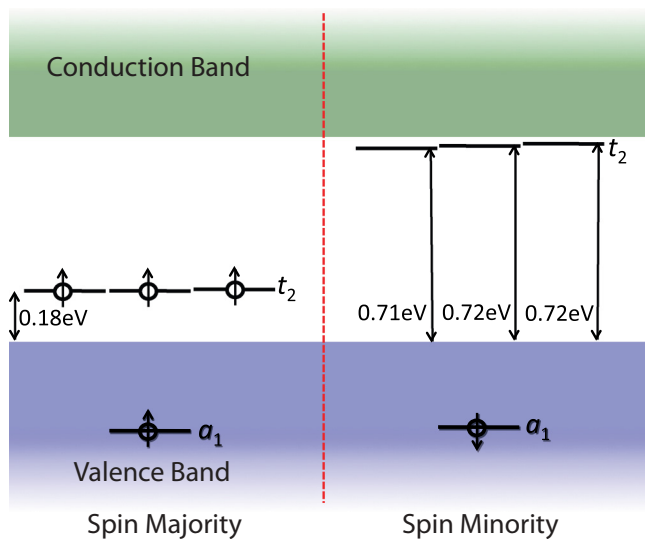


FIG. 6. (Color online) Single-particle states associated with the -1 charge state of the germanium vacancy.

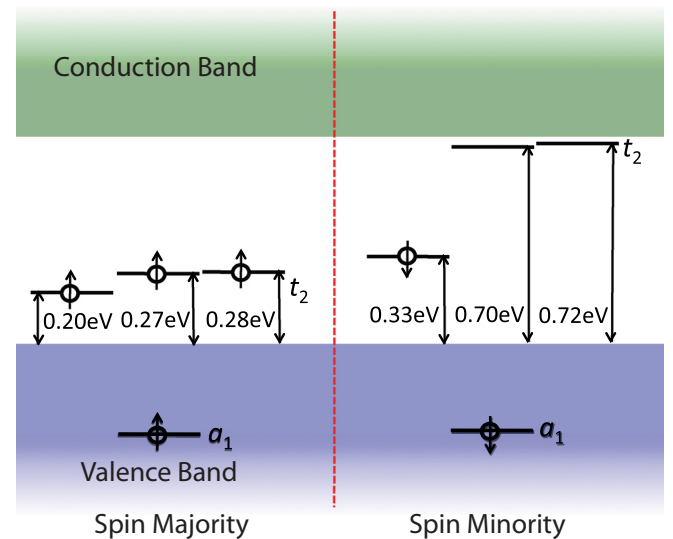


FIG. 7. (Color online) Single-particle states associated with the -2 charge state of the germanium vacancy.

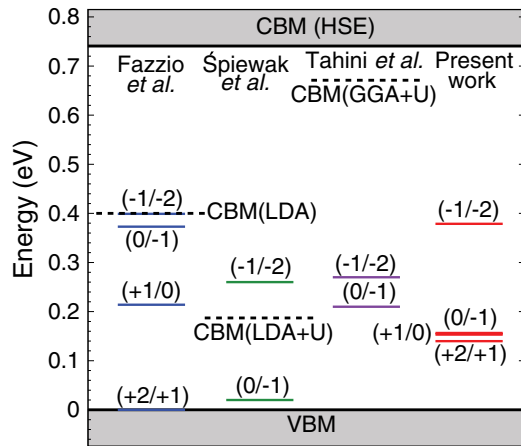


FIG. 8. (Color online) Comparison of the defect levels found in different calculations for the germanium vacancy, including Fazio *et al.*,<sup>21</sup> Spiewak *et al.*,<sup>22</sup> Tahini *et al.*,<sup>23</sup> and our present screened hybrid functional results (HSE formalism with 30% Hartree-Fock mixing). The dashed lines represent the position of the CBM in the respective calculations.

Figure 8 shows the location of the charge-state transition levels obtained in the previous computational studies,<sup>21–23</sup> compared with the results of the present work. The main computational differences between our calculations and the previous ones are that we have used hybrid functionals and spin-polarized calculations. Fazio *et al.*<sup>21</sup> used LDA but altered the germanium pseudopotential in an attempt to correct the band gap (which would otherwise be negative, in LDA). They did not consider spin polarization. Spiewak *et al.* used the LDA +  $U$  approach to correct the band gap.<sup>22</sup> As seen in Fig. 8, even with these corrections the germanium band gap is still severely underestimated. Very recently, Tahini *et al.*<sup>23</sup> used GGA +  $U$  and by tuning the  $U$  and  $J$  parameters obtained a band gap of 0.67 eV, in satisfactory agreement with experiment. Spin polarization was apparently not included.

Comparing our results to the study by Spiewak *et al.*,<sup>22</sup> we find a similar spacing between the (0/−1) and (−1/−2) transition levels. As noted above, this spacing is related to intraorbital repulsion, and the use of spin-polarized calculations is apparently essential for producing this result: Fazio *et al.*<sup>21</sup> and Tahini *et al.*<sup>23</sup> find a much smaller spacing in the absence of spin polarization. Our results differ from those of Spiewak *et al.*<sup>22</sup> and Tahini *et al.*<sup>23</sup> in that those LDA +  $U$  and GGA +  $U$  calculations did not find the (+2/+1) or (+1/0) transition levels to lie within the band gap. In the LDA +  $U$  calculations<sup>22</sup> this could be attributed to the very small band gap (0.19 eV), which does not allow for these defect levels to emerge into the band gap, but in GGA +  $U$ ,<sup>23</sup> which produced a gap of 0.67 eV, the lack of stability of the +1 and +2 charge states is more difficult to understand. We observe that the GGA +  $U$  results<sup>23</sup> were obtained by applying  $U = 0.4$  eV and  $J = 4.0$  eV to the germanium  $p$  states. The application of the DFT +  $U$  formalism to  $p$  states is not entirely justified, in our opinion;<sup>57</sup> in addition, the chosen  $U$  and  $J$  values do not adhere to the typical pattern where  $U \gg J$ . We also note that all of the calculations performed by Spiewak *et al.*<sup>22</sup> and Tahini

*et al.*<sup>23</sup> were done using a 64-atom supercell. As noted above, we found the use of a 216-atom supercell to be important.

Comparing our results for the vacancy transition levels to the calculations by Fazio *et al.*,<sup>21</sup> we note that our calculations produce a 0.02-eV spacing between the (+2/+1) and (0/−1) transition levels, while Fazio *et al.* found a 0.37-eV spacing. This is again most likely due to their use of non-spin-polarized calculations, since this will introduce an intraorbital electron-electron repulsion when going from the +1 to the 0 charge state. In our calculations, we find that it costs less energy to add the second electron to a different  $t_2$  state, while in the calculations by Fazio *et al.* spin polarization effects were ignored, so the second electron was just added to the same  $t_2$  state, thus creating a doubly occupied  $t_2$  state in the neutral charge state. This explains the large discrepancy between the spacing of the (+2/+1) and (+1/0) transition levels in our calculations compared to those by Fazio *et al.*

### 3. Comparison with the silicon vacancy and with experimental activation energies

It is informative to compare our calculated formation energies for the vacancy in germanium (Fig. 5) with formation energies for the vacancy in silicon, which we have calculated here using the same methodology. Figure 9 is designed to allow for easy comparison between the vacancy formation energies in the two materials. The associated charge-state transition levels for the silicon vacancy are shown in Fig. 10.

Two key features emerge:

(1) The formation energy of the germanium vacancy is lower than that of the silicon vacancy for the entire range of Fermi levels, making it significantly more likely that vacancies will form in germanium. Note that vacancy concentrations are related to formation energies through Eq. (1). Therefore, vacancies will be much more prevalent in germanium. This is consistent with the smaller activation enthalpy observed for vacancy-assisted self-diffusion in germanium,<sup>58</sup> compared with silicon.<sup>59</sup>

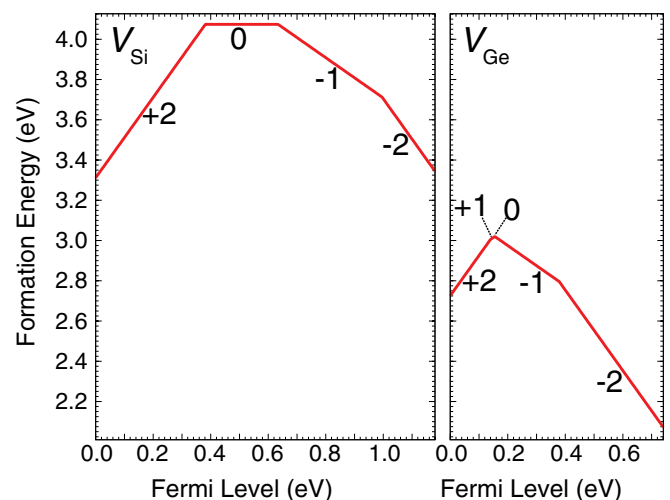


FIG. 9. (Color online) Calculated formation energy of the vacancy in silicon and germanium. The Fermi level is referenced to the respective VBM.

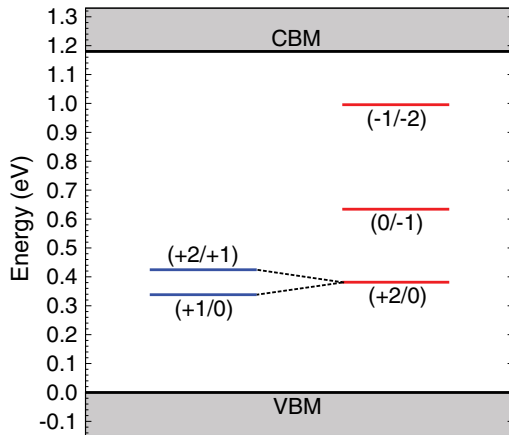


FIG. 10. (Color online) Charge-state transition levels associated with the vacancy in silicon. The red levels on the right are associated with the thermodynamically stable charge states, while the blue levels on the left are associated with the unstable  $+1$  charge state.

In addition, we can compare our formation energy results with the experimentally determined activation energies.<sup>58,59</sup> This was done by extracting approximate Fermi-level positions based on the temperatures in the experimental studies.<sup>58,59</sup> If we combine this with previously determined vacancy migration barriers in germanium (0.1 eV)<sup>60</sup> and silicon (0.5 eV),<sup>61</sup> we find activation enthalpies of 3.0 eV for germanium and 4.6 for silicon. This is in remarkable agreement with the experimental values of 3.1 eV (germanium)<sup>58</sup> and 4.8 eV (silicon).<sup>59</sup>

(2) Unlike silicon the  $+1$  charge state of the vacancy is stable in germanium (although only over a very small range of Fermi levels). Our calculations for silicon show that the  $+1$  charge state is never thermodynamically stable, characteristic of a negative- $U$  center. The calculated energy difference between the  $(+2/+1)$  and  $(+1/0)$  transitions is  $U = -0.09$  eV (see Fig. 10). Experimentally, the fact that the  $+1$  charge state of the silicon vacancy is not stable has indeed been observed using DLTS,<sup>62</sup> with a measured value of  $U = -0.08$  eV, in very good agreement with our calculations.

At first sight, the relative spacings of the charge-state transition levels of the vacancy are very different in silicon and germanium (Fig. 9). We suggest that the difference can be mainly attributed to the different behavior of the neutral charge state. In germanium, the atomic structures of the  $+2$ ,  $+1$ ,  $0$ , and  $-1$  charge states are quite similar; i.e., the atomic

relaxations do not drastically change as electrons are added to the  $t_2$  spin-up states (Fig. 6). But in silicon the neutral charge state exhibits distinctly larger relaxations, indicative of extensive rebonding and resulting in a lowering of the energy of this charge state relative to the other charge states. This can be viewed as a Jahn-Teller distortion which lowers the two occupied  $t_2$  eigenvalues with respect to the unoccupied one. This is responsible for the much larger spacing of the  $(+1/0)$  and  $(0/-1)$  transition levels in silicon compared to germanium. Why this rebonding in the neutral charge state occurs in silicon and not in germanium is an interesting question to which we do not have an answer.

#### IV. CONCLUSIONS

We have performed a detailed computational study of DBs and vacancies in germanium using screened hybrid functionals. We find that the DB is always negatively charged, with charge-state transition levels below the VBM. This explains the inability to detect germanium DBs with ESR. Our results are in agreement with published ESR data on germanium DBs at  $\text{Si}_{1-x}\text{Ge}_x\text{-SiO}_2$  interfaces. The negatively charged DB leads to a host of problems for MOSFETs, including threshold voltage shifts, reduced carrier concentration, and carrier scattering in the channel. Additionally, hydrogen is unable to passivate this defect, since hydrogen, too, is exclusively negatively charged in germanium.

For the germanium vacancy we have calculated defect transition levels that are in good agreement with experimental results, where available, in some cases enabling a specific assignment for the charge states involved in the transition. Our calculated formation energies indicate that vacancies in germanium are much more prevalent than in silicon. For both germanium and silicon our calculated energies are in excellent agreement with values extracted from self-diffusion experiments.

#### ACKNOWLEDGMENTS

We acknowledge fruitful discussions with P. Broqvist and A. Pasquarello, as well as support from the Semiconductor Research Corporation (Task No. 1867.001). We also made use of the California Nanosystems Institute Computing Facility under NSF Grant No. CHE-0321368 and the Ranger supercomputer from the TeraGrid computing resources supported by the NSF under Grant No. DMR070072N.

<sup>1</sup>C. O. Chui, S. Ramanathan, B. B. Triplett, P. McIntyre, and K. C. Saraswat, *IEEE Electron Device Lett.* **23**, 473 (2002).

<sup>2</sup>A. Ritenour, A. Khakifirooz, D. A. Antoniadis, R. Z. Lei, W. Tsai, A. Dimoulas, G. Mavrou, and Y. Panayiotatos, *Appl. Phys. Lett.* **88**, 132107 (2006).

<sup>3</sup>D. P. Brunco, B. De Jaeger, G. Eneman, J. Mitard, G. Hellings, A. Satta, V. Terzieva, L. Souriau, F. E. Leys, G. Pourtois, M. Houssa, G. Winderickx, E. Vrancken, S. Sioncke, K. Opsomer, G. Nicholas, M. Caymax, A. Stesmans, J. Van Steenberghe, P. W. Mertens, M. Meuris, and M. M. Heyns, *J. Electrochem. Soc.* **155**, H552 (2008).

<sup>4</sup>S. J. Whang, S. J. Lee, F. Gao, N. Wu, C. X. Zhu, J. S. Pan, L. J. Tang, and D. L. Kwong, Technical Digest—International Electron Devices Meeting (IEEE, New York, 2004), p. 307.

<sup>5</sup>H. Shang, K. L. Lee, P. Kozlowski, C. D'Emic, I. Babich, E. Sikorski, M. K. Jeong, H. H. P. Wong, K. Guarini, and N. Haensch, *IEEE Electron Device Lett.* **25**, 135 (2004).

<sup>6</sup>W. P. Bai, N. Lu, A. Ritenour, M. L. Lee, D. A. Antoniadis, and D. L. Kwong, *IEEE Electron Device Lett.* **27**, 175 (2006).

<sup>7</sup>S. T. Pantelides, *Deep Centers in Semiconductors: A State-of-the-Art Approach*, 2nd ed. (Gordon and Breach, Philadelphia, 1992).

- <sup>8</sup>V. V. Afanas'ev, Y. G. Fedorenko, and A. Stesmans, *Appl. Phys. Lett.* **87**, 032107 (2005).
- <sup>9</sup>A. Stesmans, *Phys. Rev. Lett.* **70**, 1723 (1993).
- <sup>10</sup>A. Stesmans, *Appl. Phys. Lett.* **68**, 2076 (1996).
- <sup>11</sup>A. Stesmans, P. Somers, and V. V. Afanas'ev, *Phys. Rev. B* **79**, 195301 (2009).
- <sup>12</sup>A. Stesmans, P. Somers, and V. V. Afanas'ev, *Microelect. Eng.* **86**, 1621 (2009).
- <sup>13</sup>A. Stesmans, P. Somers, and V. V. Afanas'ev, *J. Phys.: Condens. Matter* **21**, 122201 (2009).
- <sup>14</sup>V. V. Afanas'ev, M. Houssa, A. Stesmans, L. Souriau, R. Loo, and M. Meuris, *Appl. Phys. Lett.* **95**, 222106 (2009).
- <sup>15</sup>M. Houssa, G. Pourtois, M. Caymax, M. Meuris, M. M. Heyns, V. V. Afanas'ev, and A. Stesmans, *Appl. Phys. Lett.* **93**, 161909 (2008).
- <sup>16</sup>J. R. Weber, A. Janotti, P. Rinke, and C. G. Van de Walle, *Appl. Phys. Lett.* **91**, 142101 (2007).
- <sup>17</sup>P. Broqvist, A. Alkauskas, and A. Pasquarello, *Phys. Rev. B* **78**, 075203 (2008).
- <sup>18</sup>P. Broqvist, A. Alkauskas, and A. Pasquarello, *Materials Sci. Semiconductor Proc.* **11**, 226 (2008).
- <sup>19</sup>P. Broqvist, A. Alkauskas, and A. Pasquarello, *AIP Conf. Proc.* **1199**, 81 (2010).
- <sup>20</sup>J. P. Perdew, M. Ernzerhof, and K. Burke, *J. Chem. Phys.* **105**, 9982 (1996).
- <sup>21</sup>A. Fazzio, A. Janotti, A. J. R. da Silva, and R. Mota, *Phys. Rev. B* **61**, R2401 (2000).
- <sup>22</sup>P. Śpiewak, J. Vanhellefont, K. Sueoka, K. J. Kurzydowski, and I. Romandic, *J. Appl. Phys.* **103**, 086103 (2008).
- <sup>23</sup>H. Tahini, A. Chroneos, R. W. Grimes, U. Schwingenschlögl, and H. Bracht, *Appl. Phys. Lett.* **99**, 072112 (2011).
- <sup>24</sup>W. G. Aulbur, L. Jönsson, and J. W. Wilkins, in *Solid State Physics Vol. 54*, edited by E. Ehrenreich and F. Spaepen (Academic Press, San Diego, 2000), p. 2.
- <sup>25</sup>D. L. Trueblood, *Phys. Rev.* **161**, 828 (1967).
- <sup>26</sup>P. Penning, *Philips Res. Rep.* **13**, 17 (1958).
- <sup>27</sup>A. Hiraki and Y. Suita, *Technol. Rep. Osaka Univ.* **15**, 65 (1965).
- <sup>28</sup>L. F. Konorova, *Sov. Phys. Solid State.* **10**, 2233 (1969).
- <sup>29</sup>J. Slotte, S. Kilpeläinen, F. Tuomisto, J. Räisänen, and A. Nylandsted Larsen, *Phys. Rev. B* **83**, 235212 (2011).
- <sup>30</sup>H. Hässlein, R. Sielemann, and C. Zistl, *Phys. Rev. Lett.* **80**, 2626 (1998).
- <sup>31</sup>H. Hässlein, R. Sielemann, and C. Zistl, *Mater. Sci. Forum* **59**, 258 (1997).
- <sup>32</sup>C. Zistl, R. Sielemann, H. Hässlein, S. Gall, D. Bräunig, and J. Bollmann, *Mater. Sci. Forum* **53**, 258 (1997).
- <sup>33</sup>J. R. Weber, A. Janotti, and C. G. Van de Walle, *Microelect. Eng.* **86**, 1756 (2009).
- <sup>34</sup>F. Oba, A. Togo, I. Tanaka, J. Paier, and G. Kresse, *Phys. Rev. B* **77**, 245202 (2008).
- <sup>35</sup>J. L. Lyons, A. Janotti, and C. G. Van de Walle, *Appl. Phys. Lett.* **95**, 252105 (2009).
- <sup>36</sup>W. Kohn and L. J. Sham, *Phys. Rev.* **140**, A1133 (1965).
- <sup>37</sup>J. Heyd, G. E. Scuseria, and M. Ernzerhof, *J. Chem. Phys.* **118**, 8207 (2003).
- <sup>38</sup>J. Heyd, G. E. Scuseria, and M. Ernzerhof, *J. Chem. Phys.* **124**, 219906 (2006).
- <sup>39</sup>G. Kresse and J. Furthmüller, *Phys. Rev. B* **54**, 11169 (1996).
- <sup>40</sup>G. Kresse and D. Joubert, *Phys. Rev. B* **59**, 1758 (1999).
- <sup>41</sup>M. Marsman, J. Paier, A. Stroppa, and G. Kresse, *J. Phys.: Condens. Matter* **20**, 064201 (2008).
- <sup>42</sup>J. Paier, M. Marsman, K. Hummer, G. Kresse, I. C. Gerber, and G. G. Ángyán, *J. Chem. Phys.* **124**, 154709 (2006).
- <sup>43</sup>P. E. Blöchl, *Phys. Rev. B* **50**, 17953 (1994).
- <sup>44</sup>C. G. Van de Walle and J. Neugebauer, *J. Appl. Phys.* **95**, 3851 (2004).
- <sup>45</sup>C. Freysoldt, J. Neugebauer, and C. G. Van de Walle, *Phys. Rev. Lett.* **102**, 016402 (2009).
- <sup>46</sup>M. Lannoo and J. Bourgoin, *Point Defects in Semiconductors I: Theoretical Aspects* (Springer-Verlag, Berlin, 1981); *Point Defects in Semiconductors II: Experimental Aspects* (Springer-Verlag, Berlin, 1983).
- <sup>47</sup>P. M. Mooney, in *Identification of Defects in Semiconductors*, edited by M. Stavola, *Semiconductors and Semimetals Vol. 51B* (Academic, San Diego, 1999), p. 93.
- <sup>48</sup>C. G. Van de Walle and R. A. Street, *Phys. Rev. B* **49**, 14766 (1994).
- <sup>49</sup>B. Shin, J. R. Weber, R. D. Long, P. K. Hurley, C. G. Van de Walle, and P. C. McIntyre, *Appl. Phys. Lett.* **86**, 1756 (2009).
- <sup>50</sup>A. Dargys and J. Kundrotas, *Handbook on Physical Properties of Ge, Si, GaAs and InP* (Science and Encyclopedia, Vilnius, 1994).
- <sup>51</sup>P. W. Anderson, *Phys. Rev. Lett.* **34**, 953 (1975).
- <sup>52</sup>C. G. Van de Walle and R. M. Martin, *Phys. Rev. B* **34**, 5621 (1986).
- <sup>53</sup>V. V. Afanas'ev, A. Stesmans, L. Souriau, R. Loo, and M. Meuris, *Appl. Phys. Lett.* **94**, 172106 (2009).
- <sup>54</sup>A. Dimoulas, P. Tsipas, A. Sotiropoulos, and E. K. Evangelou, *Appl. Phys. Lett.* **89**, 252110 (2006).
- <sup>55</sup>C. G. Van de Walle, J. R. Weber, and A. Janotti, *Thin Solid Films* **517**, 144 (2008).
- <sup>56</sup>M. J. Puska, S. Pöykkö, M. Pesola, and R. M. Nieminen, *Phys. Rev. B* **58**, 1318 (1998).
- <sup>57</sup>A. Janotti and C. G. Van de Walle, *Phys. Status Solidi B* **248**, 799 (2011).
- <sup>58</sup>E. Hüger, U. Tietze, D. Lott, H. Bracht, D. Bougeard, E. E. Haller, and H. Schmidt, *Appl. Phys. Lett.* **93**, 162104 (2008).
- <sup>59</sup>H. Bracht, E. E. Haller, and R. Clark-Phelps, *Phys. Rev. Lett.* **81**, 393 (1998).
- <sup>60</sup>H. M. Pinto, J. Coutinho, V. J. B. Torres, S. Oberg, and P. R. Briddon, *Mat. Sci. Semiconductor Proc.* **9**, 498 (2006).
- <sup>61</sup>G. D. Watkins, *Mater. Res. Soc. Symp. Proc.* **469**, 139 (1997), and references therein.
- <sup>62</sup>G. D. Watkins and J. R. Troxell, *Phys. Rev. Lett.* **44**, 593 (1980).